

A WAVELET APPROACH FOR DETERMINING A SURFACE COVERED WITH AIRBORNE LIDAR POINTS

Jaan-Rong TSAY

Associate Professor, Department of Geomatics
National Cheng Kung University
1 University Road, Tainan, Taiwan
Tel: (886)-6-2370876 ext. 838 Fax: (886)-6-2375764
E-mail: tsayjr@mail.ncku.edu.tw

Cheng Wei Yen

M.Sc., Department of Geomatics, National Cheng Kung University
1 University Road, Tainan, Taiwan

KEY WORDS: Wavelet, Surface Reconstruction, Fractal, LiDAR

ABSTRACT: This paper presents a new approach for reconstructing object surface covered with 3D points. It utilizes the 2D Daubechies scaling functions of 3rd order, which can describe fractal geometry, to formulate the observation equation for each point. The linear system is then solved by the least-squares adjustment (LSA) and the reconstructed surface can then be generated. To overcome the ill-posed problem which often emerges in LSA, we employ a from-coarse-to-fine strategy and use the pseudo observations designed on dyadic points, called PHO (Pseudo Height Observations) and POI (Pseudo Observations by Interpolation). Moreover, a full-automated weighting model is proposed to eliminate the so-called Gibbs effect. It reduces the weights of the points whose absolute residuals are larger than twice the a priori height accuracy of the LiDAR point. Tests are done by using airborne LiDAR points. They verify that the artifacts can be completely eliminated by adopting the pseudo observations and the weighting model. While the dyadic points have approximately the point interval of LiDAR points, the a posteriori standard deviations of unit weight of our tests are about $\pm 20\sim 23\text{cm}$ which are all to the extents of the a priori height accuracy, $\pm 25\text{cm}$.

1. INTRODUCTION

Especially in the past decade, the technique of light detection and ranging (LiDAR) becomes a well-known method for fast acquisition of precise coordinates of densely distributed 3D points on surfaces of interest objects. It is widely utilized in diverse applications, e.g. 3D cyber city modeling or generation of virtual environment. A key advantage of the so-called LiDAR-grammetry is its ability on *fast acquisition* of precise point cloud positions in 3D object space. Nevertheless, LiDAR-grammetry still has some very critical disadvantages:

- (1) Unavoidable data errors cannot be detected and corrected without the corresponding a priori information or overlaying other data sources in the laser scanned area such as high-resolution (satellite or aerial) images or digital thematic maps or the overlapped LiDAR data scanned from other strips or other stations. Briefly to say, only LiDAR itself has completely no reliability.
- (2) LiDAR points are almost always not located on surface features of interest objects.
- (3) The resolution of LiDAR data is still limited until now.

Therefore, LiDAR should and must be integrated with other geomatic sciences and techniques in order to become a really powerful and applicable method for fast acquisition of GIS and space data with acceptable data quality (inclusive of accuracy and reliability).

This paper aims at another basic processing in LiDAR-grammetry, namely on object surface reconstruction by using the dense 3D point cloud covered on an interest surface. The dense 3D point cloud data can be acquired e.g. by laser scanning or digital photogrammetry or GPS.

For the present, the techniques for object surface reconstruction by using the dense 3D point cloud could be roughly categorized into two fields: (1) generation of a complex surface by connecting simple basic geometry primitives, and (2) surface reconstruction based on Euclidean geometry or non-Euclidean geometry such as fractal geometry. In the first field, the often used simple primitives are a triangle or a grid or a volume element (voxel) in 3D space. The constructive solid geometry (CSG) belongs to the first field. CSG can present a more complex surface by using high-order surface primitives, but the degree of complexity of the surface is still restricted by the adopted primitives (You et al., 2003).

The techniques in the second category can generate a surface with higher degree of complexity and discontinuity by using some surface functions and mathematical parameters such as Bezier surface and B-spline surface (Hill, 2000). For instance, Busé and Galligo (2004) adopted semi-implicit representation of algebraic surfaces. Anca et al. (2004) used spherical implicit functions for interactive modeling a surface. Xie et al. (2003) presented a method for piecewise C/sup 1/ continuous surface reconstruction of noisy point clouds via local implicit quadric regression. The non-Euclidean geometry formulates surfaces in non-orthogonal Euclidean spaces (Hill, 2000). Object surfaces are generated by some stochastic models and fractal dimension (Peitgen and Saupe, 1988).

Most methods in the afore-mentioned two fields still have some limitations. They only describe a piecewise smooth and continuous surface. Some of them cannot present a fractal surface. For example, Hoppe et al. (1992) reconstructed surfaces from unorganized points by utilizing iso-surfaces and the principle of marching cubes (Lorensen and Cline, 1987). Carr et al. (2003) applied the radial basis functions (RBF) to reconstruct smooth surface from noisy range data.

This paper presents a wavelet approach for determining a complex 3D surface covered with airborne LiDAR points. The surface can be locally continuous, discontinuous, smooth, rough, regular, irregular, fractal, or non-fractal. Briefly to say, it is a real surface. We utilize the 2D Daubechies scaling function of 3rd order to define a surface function. In fact, the Daubechies scaling functions and wavelets display a fractal geometry (Kaiser, 1994).

2. SURFACE FUNCTION FORMULATED BY WAVELETS

Let $f(x, y)$ be a surface function of two variables x and y . $f(x, y)$ is a continuous single-valued real function. It can be approximately described in a multi-resolution manner according to the wavelet theory by the following equation:

$$A_j f(x, y) = \sum_{k=-1}^{2^j(M-1)-1} \sum_{l=-1}^{2^j(N-1)-1} c_{k,l}^j \cdot \phi_{p,j,k,l}(x, y) \quad (1)$$

where j is a dilation parameter of the Daubechies scaling function ϕ_p of p -th order. In this paper, $p=3$ is adopted. In the computation area, 3D object points with horizontal coordinates (X_i, Y_i) are mapped linearly into the interval of $0 \leq x_i \leq M-1$ and $0 \leq y_i \leq N-1$, $\forall i$. k and l are translation parameters in the x - and y -direction, respectively. $c_{k,l}^j$ is the scaling coefficient for the scaling function $\phi_{p,j,k,l}$.

3. OBSERVATION EQUATIONS

The airborne LiDAR provides 3D points with the coordinates (x_i, y_i, z_i) , where z_i is equal to the original height Z_i determined by LiDAR. These 3D points are assumed to cover a surface, on which a point at (x_i, y_i) has only one height value z_i . The well-known least-squares adjustment (LSA) is applied here to determine a best fitting surface. In that processing step, the following observation equation is given for each point.

$$z_i(x_i, y_i) + v_i = A_j f(x_i, y_i) = \sum_{k=-1}^{2^j(M-1)-1} \sum_{l=-1}^{2^j(N-1)-1} c_{k,l}^j \cdot \phi_{p,j,k,l}(x_i, y_i) \quad (2)$$

where v_i is the residual of the height observation z_i . The function value $\phi_{p,j,k,l}(x_i, y_i)$ can be computed. Therefore, the linear equation only has the unknowns $c_{k,l}^j$. They can be determined by LSA.

4. ILL-POSED PROBLEM AND ITS SOLUTION

The airborne LiDAR produces very dense 3D points on different scanning lines. These points are not uniformly distributed in 3D space, i.e. the point interval is not constant in the entire computation area. The Daubechies scaling functions $\phi_{p,j,k,l}(x, y)$ are compactly supported. That means the function value $\phi_{p,j,k,l}(x, y)$ is equal to or very near to zero for any point which is located outside the support or near the support boundary, respectively. On a resolution level, if no point is located inside the support or points are only located near the support boundary, the corresponding row (and column) vector for that unknown $c_{k,l}^j$ in the normal matrix is then equal to or near a zero vector. The so-called ill-posed problem emerges.

In order to solve the before-mentioned and often emerged ill-posed problem, a from-coarse-to-fine strategy is adopted. The approach starts from the coarser level, namely a smaller j and a larger interval between neighboring dyadic points.

In that case, the normal matrix is positive definite and all unknowns $c_{k,l}^j$ can be solved. While all coefficients $c_{k,l}^j$ are known, the approximation values on all dyadic points at the next finer level can be computed by the equation (3). They are called the pseudo height observations (PHOs) in this paper.

$$PHO_j = A_j f(x, y) = \sum_{k=-1}^{2^j(M-1)-1} \sum_{l=-1}^{2^j(N-1)-1} c_{k,l}^j \cdot \phi_{p,j,k,l}(x, y) \quad (3)$$

On the other hand, another pseudo observations are computed for all dyadic points at that next finer level. The nearest neighborhood interpolation is computed for each dyadic point. The neighborhood is a circle region centered at a dyadic point and with a radius σ_{xy} , where σ_{xy} denotes the a priori horizontal accuracy of LiDAR points. If there is no LiDAR point inside the neighborhood, the pseudo observation PHO is adopted for that dyadic point. Otherwise, the interpolated value named POI is used as the pseudo observation for that dyadic point. In other word, each dyadic point has a either POI or PHO as its pseudo observation. Both are called POI and PHO points, respectively. They are used together with all original LiDAR points in LSA at that level. In this manner, a precise surface at the finest level can then be determined.

5. TEST DATA

In order to test the efficiency of our approach, airborne LiDAR data are used. They are acquired by the Optech ALTM 3070 system. The scanning density is about one points per meter. These LiDAR points have the a priori horizontal and vertical accuracy of about $\pm 1m$ and ± 25 cm, respectively. Figure 1 illustrates our three test areas A, B, and C. Table 1 shows they contain different types of surfaces such as buildings, trees, semi-spherical roof, etc.

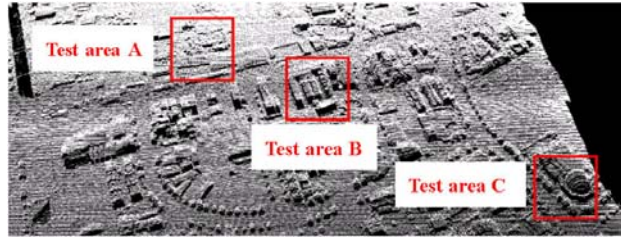


Figure 1. LiDAR points in the test areas A, B, and C.

Table 1. Illustration of the test areas A, B, and C

	Test area A	Test area B	Test area C
LiDAR point cloud			
Google Earth image in the test area			
Number of LiDAR points	10921	9578	10047
Horizontal dimension	$\Delta X \cong \Delta Y \cong 100$ m	$\Delta X \cong \Delta Y \cong 100$ m	$\Delta X \cong \Delta Y \cong 100$ m
Height range	$\Delta Z \cong 14.5$ m	$\Delta Z \cong 28.1$ m	$\Delta Z \cong 30.5$ m

Table 2. Statistic figures of the computations in the test area B for the levels $j=0$ to $j=3$.

j	Groundel size (m)	Number of unknowns	Number of POI points	Number of PHO points	$\pm \hat{\sigma}_0 (m)$
0	10	121	×	×	3.73
1	5	441	×	×	2.64
2	2.5	1681	1645	36	1.97
3	1.25	6561	6439	122	1.50

Table 3. Some statistic figures of the computations in the test area B for the levels $j=2$ and $j=3$

j	Number of unknowns	Number of POI points	Number of PHO points	W_1	W_2	$\pm \hat{\sigma}_0 (m)$
2	1681	1645	36	1	1	1.97
2*				1	0.0076	0.30
3	6561	6439	122	1	1	1.50
3*				1	0.0072	0.23

6. GIBBS EFFECT

Table 2 expresses some statistic figures of the computations in the test area B from the coarse level $j=0$ to the fine level $j=3$. The groundel size means the distance between neighboring dyadic points. The finer the resolution is, the better the fitting accuracy of the determined surface is. In case of $j=3$, the a posteriori standard deviation is $\pm 1.5m$ which is significantly much larger than the a priori height accuracy of $\pm 25cm$. Moreover, The determined surfaces also show clearly that more detailed surface structures are reconstructed with finer resolution. Nevertheless, unreasonably large undulation surfaces are reconstructed near local discontinuous surface such as walls, boundary of high trees, electric poles, etc. It is the well-known Gibbs phenomenon.

7. WEIGHTING MODEL

In order to eliminate the Gibbs effect, we propose a full-automated weighting model to reduce the weights of the LiDAR points whose absolute residuals are larger than twice the a priori height accuracy of the LiDAR data, namely $|v_i| > 2\sigma_z$. The equation (4) shows their weights, where $\hat{\sigma}_i$ denotes the ideal a posteriori standard deviation, e.g. $\hat{\sigma}_i = \sigma_z = \pm 25$ cm in our tests. The number of such LiDAR points with larger residual is r and the sum of their square residuals is denoted by $[v^2]_r^e$. The total number of LiDAR points and POI points and PHO points as well is expressed by n . These LiDAR points with larger residuals own the weight p . The other points have the unit weights.

$$p = \hat{\sigma}_i^2 \cdot \frac{r}{[v^2]_r^e} \cdot \frac{(n-u)}{n} \quad (4)$$

8. TEST RESULTS AND ANALYSIS

Table 3 shows some statistic figures of the computations in the test area B for the levels $j=2$ and $j=3$, where * denotes the reconstructions using the weighting function (4); W_1 and W_2 are the weights of observations with $|v| \leq 2\sigma_z$ and $|v| > 2\sigma_z$, respectively; σ_z denotes the a priori height accuracy ($\sigma_z = \pm 25cm$ in our cases). Apparently, the a posteriori standard deviation of unit weight is successfully reduced to $\hat{\sigma}_0 = \pm 23cm$ after the afore-mentioned weighting model is utilized. Figure 2 illustrates the location of the LiDAR points with larger residuals, namely with the weight W_2 , in test area B for $j=2$ and $j=3$. Apparently, almost all of those LiDAR points with larger residuals $|v| > 2\sigma_z$ are more nearby located at break-lines than the case at coarser level. Similar results are also obtained in another two test areas A and C. They indicate that our approach has the potential for detecting local discontinuous structures on object surfaces.

Moreover, the test results verify that the afore-mentioned weighting model really can eliminate the Gibbs effect. Figure 3 shows the reconstructed surfaces with $j=2$ and $j=3$ after the weighting model is adopted. Similar results are also obtained in the test areas A and C. They demonstrate the good ability of our approach for simultaneously reconstructing different types of surfaces such as local plane, crown canopy of trees, semi-spheric roof, etc., in a computation.

Table 4 and Table 5 show the statistic figures of the computations in the test area A and C for the levels $j=0$ to $j=3$. They demonstrate similar results as to the case in the test area B as shown in Table 3. While the interval of dyadic

points reaches the level of LiDAR point interval, the a posteriori standard deviations of unit weight in the test areas are about $\pm 20\text{cm}$, $\pm 23\text{cm}$, $\pm 22\text{cm}$. They are all to the extents of the a priori height accuracy, $\pm 25\text{cm}$.



Figure 2. Black points denote the observation points with the weight W_2 in the test area B for $j=2$ (left) and $j=3$ (right)

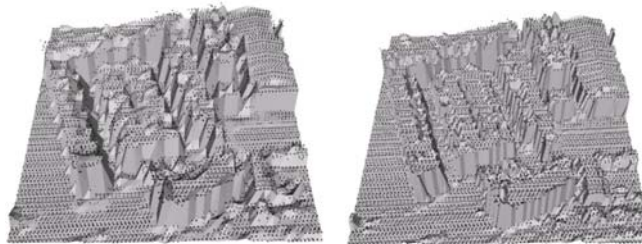


Figure 3. LiDAR points draped on the reconstructed surface of the level $j=2$ (left) and $j=3$ (right) in the test area B

Table 4. Statistic figures of the computations in the test area A for the levels $j=0$ to $j=3$

j	Groundel size (m)	Number of unknowns	Number of POI points	Number of PHO points	W_1	W_2	$\pm \hat{\sigma}_0 (m)$
0	10	121	×	×	×	×	1.47
1	5	441	×	×	×	×	1.11
2	2.5	1681	1657	24	1	1	0.85
2*					1	0.028	0.24
3	1.25	6561	6514	47	1	1	0.57
3*					1	0.032	0.20

Table 5. Statistic figures of the reconstructions in test area C for the levels $j=0$ to $j=3$

j	Groundel size (m)	Number of unknowns	Number of POI points	Number of PHO points	W_1	W_2	$\pm \hat{\sigma}_0 (m)$
0	10	121	×	×	×	×	2.97
1	5	441	×	×	×	×	2.37
2	2.5	1681	1529	152	1	1	2.06
2*					1	0.0062	0.28
3	1.25	6561	6010	551	1	1	1.84
3*					1	0.0053	0.22

Figure 4 illustrates the reconstructed surfaces draped with the corresponding Google Earth images in these three test areas A, B, and C. The afore-mentioned concluding remarks are verified that a finer surface can be reconstructed by our approach with finer resolution, namely larger j .



Figure 4. Reconstructed surfaces draped with the corresponding Google Earth images in the test areas A, B, and C

9. CONCLUDING REMARKS

This paper presents a wavelet approach for determining a complex 3D surface covered with airborne LiDAR points. The surface can be locally continuous, discontinuous, smooth, rough, fractal, or non-fractal. We utilize the 2D Daubechies scaling function of 3rd order, which can describe fractal geometry, to write the observation equations of the point cloud. Furthermore, the linear system is solved by the least-squares adjustment and the surface can then be determined. To overcome the often emerged ill-posed problem, we employ a from-coarse-to-fine strategy and use the pseudo observations on dyadic points, namely PHO (Pseudo Height Observations) and POI (Pseudo Observations by Interpolation), to stabilize the linear system and to get the solutions.

Our experimental results show that with assistance of the pseudo observations on dyadic points, the algorithm can yield a stable solution and can meet with our basic hypotheses. Besides, we find: ① Gibbs effect: some irregular artifacts emerge around the abrupt areas of the reconstructed surface. ② points with larger residuals are largely located on abrupt areas such as walls, poles, or isolated trees. To eliminate the artifact effect, we propose a full-automated weighting model to reduce the weights of the points whose absolute residuals are higher than twice the a priori height accuracy of the LiDAR data. The results reveal that by combining the pseudo observations and the weighting model, artifacts can be completely eliminated and the a posteriori standard deviation of unit weight of the reconstructed surface can reach the same level of the height accuracy of LiDAR data points. For instance, while the interval of dyadic points reaches the level of LiDAR point interval, the a posteriori standard deviations of unit weight in our tests are about $\pm 20\sim 23\text{cm}$ and are all to the extents of the a priori height accuracy, $\pm 25\text{cm}$.

By comparing to the diverse currently available surface reconstruction algorithms, the proposed approach can handle irregular, non-smooth, and fractal signals quite well and significant surface features registered in the original discrete sample points can be clearly expressed in the reconstructed surface. After some computation parameters are manually given, without the need on any other data preprocessing, our reconstruction system can automatically reconstruct a precise, highly complex, and multi-resolution surface model from discrete LiDAR points.

ACKNOWLEDGEMENT

We sincerely appreciate the National Science Council at Executive Yuen, R.O.C. for supporting this work under the project numbers NSC94-2211-E-006-072, and the Chung Hsing Surveying Co., Ltd. for providing the airborne LiDAR data for our tests.

REFERENCES

- Anca, A., Gaildrat, V., Barthe, L., 2004. Modeling and representing surfaces: Interactive modeling from sketches using spherical implicit functions. Proceedings of the 3rd international conference on Computer Graphics, Virtual Reality, Visualization and Interaction in Africa, pp. 25-34.
- Busé, L. & Galligo, A., 2004. Using semi-implicit representation of algebraic surfaces. IEEE Transactions on Shape Modeling Applications 2004, pp. 342-345.
- Carr, J. C., Beatson, R. K., McCallum, B. C., Fright, W. R., McLennan, T. J., and Mitchell, T. J., 2003. Representation: smooth surface reconstruction from noisy range data. Proceedings of the 1st international conference on Computer Graphics and Interactive Techniques in Australasia and South East Asia, pp. 119-126.
- Hill, Francis S., 2000. Computer graphics using OpenGL, 2nd edition. ISBN: 0023548568, Prentice Hall, USA
- Hoppe, H., DeRose, T., Duchamp, T., McDonald, J., and Stuetzle, W., 1992. Surface reconstruction from unorganized points. ACM SIGGRAPH 1992, pp. 71-78.
- Kaiser, G., 1994. A Friendly Guide to Wavelets, Birkhäuser Boston.
- Lorensen, W. E. & Cline, H. E., 1987. Marching cubes: A high resolution 3D surface construction algorithm. ACM SIGGRAPH 1987, pp. 163-169.
- Optech Incorporated, 2004. ALTM 3100 System Specifications, http://www.optech.ca/pdf/Specs/specs_altm_3100.pdf
- Peitgen, H. O. & Saupe, D., 1988. The Science of Fractal Images. Springer-Verlag, New York.
- You, S., Hu, J., and Fox, P., 2003. Urban site modeling from Lidar. Proceedings of Second International Workshop on Computer Graphics and Geometric Modeling, Vol. 2668, pp. 579-588.
- Xie, H., Wang, J., Hua, J., Qin, H., and Kaufman, A., 2003. Piecewise C/sup 1/ continuous surface reconstruction of noisy point clouds via local implicit quadric regression. IEEE Transactions on Visualization 2003, pp. 91-98.